Nr. 14
31. July 2014

Leopold-Franzens-Universität Innsbruck

Preprint-Series: Department of Mathematics - Applied Mathematics

Introduction to the mathematics of computed tomography

Markus Haltmeier and Sergiy Pereverzyev Jr.

REVISED VERSION, AUGUST 2014

Technikerstraße 21a - 6020 Innsbruck - Austria
Tel.: +43 512 507 53803 Fax: +43 512 507 53898
https:\\www.applied-math.uibk.ac.at

Introduction to the mathematics of computed tomography

Markus Haltmeier and Sergiy Pereverzyev Jr.

Department of Mathematics
University of Innsbruck
Technikestraße 21a, A-6020 Innsbruck
E-mail: {markus.haltmeier,sergiy.pereverzyev}@uibk.ac.at

1 Introduction

Computed tomography (CT) is one of the most important diagnostic tools in modern medicine. While the term *computed tomography* was initially reserved for x-ray based CT scanners, it nowadays covers various non-invasive imaging technologies, where mathematics plays a major role for obtaining diagnostic images. Examples include x-ray CT, single photon emission computed tomography (SPECT), positron emission tomography (PET), magnetic resonance tomography (MRT), ultrasound tomography, electrical impedance tomography, optical imaging, as well as photoacoustic tomography and the closely related thermoacoustic tomography.

A unifying element of all tomographic applications is that only indirect information about the quantity of interest (usually modelled as a function defined on $\mathbb{R}^2$ or $\mathbb{R}^3$) can be collected when scanning the patient. Due to the modeling imperfections, measurement errors and statistical uncertainties, the data are additionally corrupted by deterministic or random noise. Such type of applications are most conveniently be studied in the framework of inverse problems, where the reconstruction problem is formulated as an operator equation

$$Y = \mathcal{K} f + \epsilon \,.$$

Here $\mathcal{K}$ is a linear or non-liner operator modeling the particular inverse problem, f is the unknown (infinite dimensional) parameter, ϵ is the noise, and Y are the given noisy data. In many medical imaging technologies the operator $\mathcal{K}$ can be modelled as a Radon transform, which maps a function to its integrals over curves or other manifolds. For example, the data in the classical x-ray CT as well as in single photon emission tomography provide approximate integrals of the unknown parameter over straight lines. In the more recent photoacoustic tomography, the underlying transform is the spherical Radon transform, which integrates the unknown function over spherical surfaces.

In this note, we highlight two prime examples of computed tomography, namely classical x-ray based CT and the more recent photoacoustic tomography. For both applications we present the underlying modeling equations. We further discuss basic mathematical results that form the foundation of the filtered backprojection algorithm, which is still the most widely used reconstruction algorithm in medical CT scanners. More extensive introductions to the mathematics of computed tomography can be found, for example, in [KS01, Kuc14, Nat01, NW01, Her09].

2 The classical Radon transform

X-ray CT is the oldest non-invasive medical imaging methodology, where mathematical reconstruction algorithms play a major role for creating slice images of some patient. Like medical radiography, it is based on the physical properties that x-rays mainly propagate along straight lines in tissue and that the spatially varying x-ray attenuation depends on the structure in the interior of the patient. However, in radiology only projection images (averages of the attenuation function over lines) are captured and displayed, whereas x-ray CT uses mathematical reconstruction algorithms combining several projection images to provide section images of the interior of the patient as final output.

The Radon transform, which maps a function defined in the Euclidian plane to its integrals over straight lines forms the mathematical basis of x-ray CT. Image reconstruction in x-ray CT therefore requires a precise understanding of the Radon transform and in particular requires methods for its analytical or numerical inversion. In 1963, Cormack [Cor63] was the first to point out the possible application of the Radon transform for medical applications. The first commercially available CT system was constructed by Hounsfield [Hou73], and the first patient brain-scan in a hospital was made in 1972. In 1979, Cormack and Hounsfield shared the Nobel Prize for Medicine and Physiology for the development of computed tomography. Later Cormack realized that the transform he studied, was already analyzed in 1917 by Johann Radon (see [Rad17]), an Austrian mathematician interested in the problem of recovering a function from its line integrals from a purely mathematical perspective. A long time before the invention of computed tomography Radon already derived an inversion formula for the transform that was later named after him. Radon itself was inspired by work of another Austrian mathematician, Paul Funk, who studied a similar problem, namely that of recovering a function on the two-dimensional sphere from its integrals over all great circles [Fun13].

2.1 Mathematical modeling of x-ray CT

For the following, let $\Omega \subset \mathbb{R}^2$ be some convex domain in the Euclidian plane modeling a slice of some human patient. We denote by $f\colon \mathbb{R}^2 \to \mathbb{R}$ the spatially varying x-ray absorption coefficient which is assumed to be supported in Ω. Suppose further, that an x-ray beam origins at some position x_0 outside of Ω, propagates along a

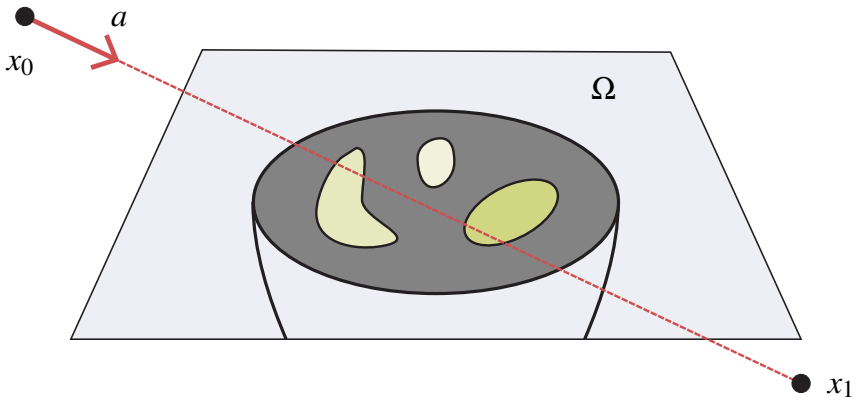

Figure 1: An x-ray is emitted at some point x_0 outside of Ω, propagates along the line L through Ω, and is finally recorded at another location x_1 outside of Ω.

straight line L and is finally recorded at another point x_1 outside of Ω; see Figure 1. We parameterize the line L by $\gamma\colon \mathbb{R} \to \mathbb{R}^2\colon t \mapsto x_0 + ta$, where $a \in \mathbb{R}^2$ is a unit vector pointing from x_0 to x_1 and denote by $I(t)$ the intensity of the x-ray beam at location $\gamma(t)$. The intensity at the source position x_0 will be denoted by I_0 and the intensity at the receiver position x_1 by I_1.

According to Beer's law, the loss of intensity in a small interval $[t, t+\Delta t]$ is approximately proportional to the intensity $I(t)$, the attenuation coefficient $f(\gamma(t))$, and the length Δt of the interval. Hence we have $I(t+\Delta t) - I(t) \approx -f\big(\gamma(t)\big)I(t)\Delta t$ and taking the limit $\Delta t \to 0$ yields the initial value problem

$$\begin{cases} \dfrac{dI}{dt}(t) = -f\big(\gamma(t)\big)I(t) & \text{for } t \in \mathbb{R} \\ I(0) = I_0\,. \end{cases}$$

Integrating this equation gives $I(t) = I_0 \exp\Big(-\int_0^t f\big(\gamma(t)\big)\mathrm{d}t\Big)$. Evaluating this expression at the special value $t_1 = |x_1 - x_0|$ (corresponding to the detector location) and using $I_1 = I(t_1)$ yields

$$\int_L f(x)\mathrm{d}s(x) := \int_0^{t_1} f(\gamma(t))\mathrm{d}t = \log\left(\frac{I_0}{I_1}\right)\,. \tag{1}$$

From (1) we conclude, that every pair of intensity I_0 emitted by some x-ray source at x_0 and intensity I_1 measured by an x-ray detector at x_1 provides the integral of f over the straight line through the points x_0 and x_1.

By varying the positions of the x-ray sources and detectors, respectively, one collects several integrals of f over different lines. The mathematical task of CT is to recover the function f from these line integrals. The first CT scanner operated in parallel beam mode. As illustrated in the left picture in Figure 2, the source and detector translate linearly, where at any instance a single line integral is collected.

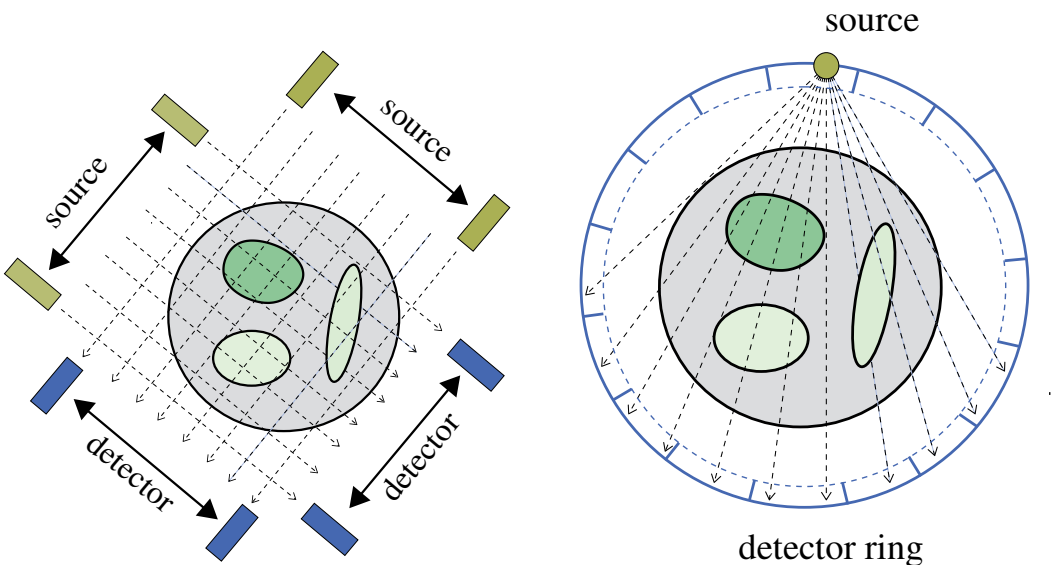

Figure 2: LEFT: In a *first generation CT scanner* a single source and detector pair is translated linearly. Subsequently the source and detector are rotated and the measurement process is repeated for different orientations. RIGHT: In modern *fourth generation CT scanner* a single source sends out a fan-shaped bunch of x-rays that are recorded with a detector ring surrounding the patient. Subsequently the source is rotated and the measurement process is repeated with different source locations.

Subsequently, the whole apparatus is rotated by a certain angle and the measurements are repeated until the whole angular range is covered. Such type of scanners are now known as first generation x-ray scanners. Modern fourth generation x-ray scanners operate in fan beam shape where a whole bunch of x-rays is emitted from a single source which rotates around the object of interest (see the right picture in Figure 2).

2.2 The Radon transform

The Radon transform, which integrates a function $f\colon \mathbb{R}^2 \to \mathbb{R}$ over all lines, forms the mathematical basis of x-ray tomography. Let us write any line in the plane in the form $L = \{s\theta + t\theta^\perp \colon t \in \mathbb{R}\}$, where $\theta \in S^1$ is a normal vector, $s \in \mathbb{R}$ is the oriented distance of the line from the origin, and let $\theta^\perp \in S^1$ denote a unit vector orthogonal to θ.

Definition 1 (Radon transform)**.** The *Radon transform* $\mathcal{R}f\colon S^1 \times \mathbb{R} \to \mathbb{R}$ of an integrable function $f\colon \mathbb{R}^2 \to \mathbb{R}$ is defined by

$$(\mathcal{R}f)(\theta, s) := \int_{\mathbb{R}} f(s\theta + t\theta^\perp)\mathrm{d}t\,.$$

For fixed $\theta \in S^1$ we call the univariate function $(\mathcal{R}f)(\theta, \cdot)\colon \mathbb{R} \to \mathbb{R}$ the linear projection of f orthogonal to θ.

By Fubini's theorem $(\mathcal{R}f)(\theta, s)$ is well defined for almost any $(\theta, s) \in S^1 \times \mathbb{R}$. We sometimes suppose that f is supported in the open unit disc $D = \{x \in \mathbb{R}^2 : |x| < 1\}$. One easily shows, that $\mathcal{R}$ then defines a linear bounded operator $\mathcal{R}\colon L^2(D) \to L^2(S^1 \times (-1, 1))$, see [Nat01].

Two main theorems

The most basic and probably most important result for the Radon transform is the Fourier slice theorem, that relates the Radon transform to the Fourier transform. For that purpose we denote by

$$(\mathcal{F}f)(\xi) := \int_{\mathbb{R}^d} f(x) e^{-i\langle \xi, x\rangle} \mathrm{d}x \qquad \text{for } \xi \in \mathbb{R}^d\,,$$

the d-dimensional Fourier transform and by $(\mathcal{F}_2 g)(\theta, \sigma) := (\mathcal{F} g(\theta, \cdot))(\sigma)$ the Fourier transform of a function $g\colon S^1 \times \mathbb{R} \to \mathbb{R}$ in the second argument.

Theorem 2 (Fourier slice theorem)**.** *For any integrable function $f\colon \mathbb{R}^2 \to \mathbb{R}$ we have*

$$(\mathcal{F}f)(\sigma\theta) = (\mathcal{F}_2\mathcal{R}f)(\theta, \sigma) \qquad \textit{for } (\theta, \sigma) \in S^1 \times \mathbb{R}\,. \tag{2}$$

Proof. This is a simple application of Fubini's theorem. In fact, by Fubini's theorem and the orthonormality of θ and $\theta^\perp$, we have

$$\begin{aligned}(\mathcal{F}_2\mathcal{R}f)(\theta, \sigma) &= \int_{\mathbb{R}} e^{-i\sigma s} \int_{\mathbb{R}} f(s\theta + t\theta^\perp)\mathrm{d}t\mathrm{d}s \\ &= \int_{\mathbb{R}}\int_{\mathbb{R}} e^{-i\langle \sigma\theta, s\theta + t\theta^\perp\rangle} f(s\theta + t\theta^\perp)\mathrm{d}t\mathrm{d}s = (\mathcal{F}f)(\sigma\theta)\,,\end{aligned}$$

where the last equality follows by the change of variables $x = s\theta + t\theta^\perp$. □

The argument $\sigma\theta$ appearing on the left hand side of (2) fills in the whole Fourier plane, which is required to invert the Fourier transform using the well known, explicit and stable Fourier inversion formula $f(x) = \frac{1}{4\pi^2}\int_{\mathbb{R}^2}(\mathcal{F}f)(\xi)e^{i\langle \xi, x\rangle}\mathrm{d}\xi$. Hence the function f can be reconstructed by means of one-dimensional Fourier transform, followed by an interpolation based on (2), and finally performing an inverse two-dimensional Fourier transform. Note however, that interpolation in the Fourier domain is a critical issue and such Fourier domain algorithms have not been very successful in early stages of CT. More recently, such type of algorithms have been improved significantly using ideas from nonuniform fast Fourier transforms [Bey95, DR93, Fes07, Fou03, GGF00, GL04, KKP09, PST01] or by gridding techniques originally developed for magnetic resonance tomography [O'S85, ST95].

While reconstruction algorithms based on the Fourier slice theorem exist, much more common are algorithms of the filtered back-projection type. Such algorithms

are based on explicit inversion formulas we shall consider next. For that purpose we denote by

$$(\mathcal{H}_2 g)(\theta, s) := \frac{1}{\pi} \int_{\mathbb{R}} \frac{g(\theta, t)}{s - t} \quad \text{for } (\theta, s) \in S^1 \times \mathbb{R}\,, \tag{3}$$

the Hilbert transform of a function $g\colon S^1 \times \mathbb{R} \to \mathbb{R}$ applied in the second argument. Here the integral is understood in the Cauchy principal value sense. The Hilbert transform is the convolution with the distribution $\mathrm{P.V.}[1/(\pi s)]$ and has the well known Fourier representation $(\mathcal{F}_2 \mathcal{H}_2 g)(\theta, \sigma) = -i \operatorname{sign}(\sigma)(\mathcal{F}_2 g)(\theta, \sigma)$. Likewise we denote by $\partial_2 g$ the derivative of g in the second argument.

Theorem 3 (Filtered back-projection type inversion formula)**.** *For any continuously differentiable function $f\colon \mathbb{R}^2 \to \mathbb{R}$ with support in D, we have*

$$\begin{aligned} f(x) &= \frac{1}{4\pi} \int_{S^1} \left(\mathcal{H}_2 \partial_2 \mathcal{R} f\right)(\theta, \langle \theta, x \rangle)\, \mathrm{d}\theta \\ &= \frac{1}{4\pi^2} \int_{S^1} \left(\int_{\mathbb{R}} \frac{(\partial_2 \mathcal{R} f)(\theta, t)}{\langle \theta, x \rangle - t} \mathrm{d}t \right) \mathrm{d}\theta \qquad \textit{for } x \in \mathbb{R}^2\,. \end{aligned} \tag{4}$$

There are several different ways to derive the important inversion formula (4); see for example [Hel80, KS01, Nat01]. Below we shall give a simple proof based on the Fourier slice theorem.

Proof of Theorem 3. By the two-dimensional Fourier inversion formula, the use of polar coordinates $\xi = \sigma\theta$, and the Fourier slice theorem we have

$$\begin{aligned} f(x) &= \frac{1}{4\pi^2} \int_{\mathbb{R}^2} (\mathcal{F} f)(\xi) e^{i\langle \xi, x \rangle} \mathrm{d}x \\ &= \frac{1}{4\pi^2} \int_{S^1} \int_0^\infty \sigma (\mathcal{F}_2 \mathcal{R} f)(\theta, \sigma) e^{i\sigma\langle \theta, x \rangle} \mathrm{d}\sigma \mathrm{d}\theta \\ &= \frac{1}{8\pi^2} \int_{S^1} \int_{\mathbb{R}} |\sigma|\, (\mathcal{F}_2 \mathcal{R} f)(\theta, \sigma) e^{i\sigma\langle \theta, x \rangle} \mathrm{d}\sigma \mathrm{d}\theta\,. \end{aligned}$$

The Fourier representations of the Hilbert transform and the derivative in the second argument show $|\sigma|\, (\mathcal{F}_2 \mathcal{R} f)(\theta, \sigma) = (\mathcal{F}_2 \mathcal{H}_2 \partial_2 \mathcal{R} f)(\theta, \sigma)$. Hence, application of the one-dimensional Fourier inversion formula yields

$$\begin{aligned} f(x) &= \frac{1}{8\pi^2} \int_{S^1} \int_{\mathbb{R}} (\mathcal{F}_2 \mathcal{H}_2 \partial_2 \mathcal{R} f)(\theta, \sigma) e^{\sigma\langle \theta, x \rangle} \mathrm{d}\sigma \mathrm{d}\theta \\ &= \frac{1}{4\pi} \int_{S^1} (\mathcal{H}_2 \partial_2 \mathcal{R} f)(\theta, \langle \theta, x \rangle) \mathrm{d}\theta\,, \end{aligned}$$

which is the first claimed inversion formula. The second inversion follows after inserting the definition of the Hilbert transform in the former. □

There exist several other explicit inversion formulas for the Radon transform (see for example [Hel80, KS01, Nat01]), which are more or less equivalent to the one of Theorem 3. The first such formula has been derived by Johann Radon in 1917 a long time before the development of computed tomography (see [Rad17]; the original paper is reprinted in the book [Hel80, pp. 177–192]). Note that Cormack and Hounsfield, the inventors of CT, had originally been unaware of the work of Radon and therefore independently (of Radon and each other) derived appropriate inversion techniques.

Dual convolution

While the filtered backprojection algorithm can be seen as a numerical implementation of (6) it is more naturally developed using a convolution identity for the dual Radon transform we shall study next. For that purpose, we denote by $(f_1 * f_2)(x) := \int_{\mathbb{R}^d} f_1(x-y) f_2(y) \mathrm{d}y$ the convolution of two functions $f_1, f_2 \colon \mathbb{R}^d \to \mathbb{R}$. When applied to functions defined on $S^1 \times \mathbb{R}$, we make the convention that it only acts in the second component. Further, we define dual Radon transform

$$\left(\mathcal{R}^\sharp g\right)(x) = \int_{S^1} g(\theta, \langle \theta, x \rangle) \mathrm{d}\theta \,,$$

for some integrable function $g \colon S^1 \times \mathbb{R} \to \mathbb{R}$. One easily shows that one has in fact the following dual property

$$\int_{S^1} \int_{\mathbb{R}} \left(\mathcal{R} f\right)(\theta, s) g(\theta, s) \mathrm{d}s \mathrm{d}\theta = \int_{\mathbb{R}^2} f(x) \left(\mathcal{R}^\sharp g\right)(x) \mathrm{d}x \,.$$

Further, the following important properties hold, which serves as the basis of the filtered backprojection algorithm we derive in the next section.

Theorem 4 (Dual convolution)**.** *Let $f \colon \mathbb{R}^2 \to \mathbb{R}$ be integrable and let $g \colon S^1 \times \mathbb{R} \to \mathbb{R}$ be C^1 with sufficient decay at infinity. Then*

(a) $\left(\mathcal{R}^\sharp g\right) * f = \mathcal{R}^\sharp \left(g * \mathcal{R} f\right)$

(b) For all $\xi \in \mathbb{R}^2$, we have $\left(\mathcal{F} \mathcal{R}^\sharp g\right)(\xi) = 2 \left|\xi\right|^{-1} \mathcal{F}_2 g \left(\xi / \left|\xi\right|, \left|\xi\right|\right)$.

(Note that the function $\mathcal{R}^\sharp g$ is in general not integrable and therefore $\mathcal{F}\mathcal{R}^\sharp g$ has to be defined in the sense of distributions.)

Proof. (a) The definition of the dual transform and Fubini's thm show

$$\begin{aligned}
\left(\mathcal{R}^\sharp g\right) * f(x) &= \int_{\mathbb{R}^2} \int_{S^1} g\left(\langle \theta, x - y \rangle\right) \mathrm{d}\theta f(y) \mathrm{d}y \\
&= \int_{S^1} \int_{\mathbb{R}} \int_{\mathbb{R}} g\left(\langle \theta, x \rangle - s\right) f(s\theta + t\theta^\perp) \mathrm{d}t \mathrm{d}s \mathrm{d}\theta \\
&= \int_{S^1} \int_{\mathbb{R}} g\left(\langle \theta, x \rangle - s\right) \mathcal{R} f(\theta, s) \mathrm{d}s \mathrm{d}\theta
\end{aligned}$$

$$= \mathcal{R}^\sharp \left(g * \mathcal{R}f\right)(x)\,.$$

(b) Suppose that $\varphi \in \mathcal{S}\left(\mathbb{R}^2\right)$ is any Schwartz function. According to the distributional definition of the Fourier transform and the Fourier slice theorem,

$$\begin{aligned}
\int_{\mathbb{R}^2} \left(\mathcal{R}^\sharp g\right)(x) \left(\mathcal{F}\varphi\right)(x)\mathrm{d}x &= \int_{S^1}\int_{\mathbb{R}} g(\theta,\sigma)\left(\mathcal{R}\mathcal{F}\varphi\right)(\theta,\sigma)\mathrm{d}\sigma\mathrm{d}\theta \\
&= \int_{S^1}\int_{\mathbb{R}} \left(\mathcal{F}g\right)(\theta,\sigma)\left(\mathcal{F}^{-1}\mathcal{R}\mathcal{F}\varphi\right)(\theta,\sigma)\mathrm{d}\sigma\mathrm{d}\theta \\
&= 2\int_{S^1}\int_{0} \left(\mathcal{F}g\right)(\theta,\sigma)\varphi(\sigma\theta)\mathrm{d}\sigma\mathrm{d}\theta \\
&= 2\int_{\mathbb{R}^2} \frac{\left(\mathcal{F}g\right)\left(\xi/\left|\xi\right|,\left|\xi\right|\right)}{\left|\xi\right|}\varphi(\xi)\mathrm{d}\xi\,.
\end{aligned}$$

This shows that $\mathcal{F}\mathcal{R}^\sharp g$ is a regular distribution and represented by the function $\xi \mapsto 2\frac{(\mathcal{F}g)(\xi/|\xi|,|\xi|)}{|\xi|}$. □

Generalization to higher dimensions

The Radon transform can easily be generalized to higher dimensions, where it maps a function $f\colon \mathbb{R}^n \to \mathbb{R}$ to its integrals $(\mathcal{R}f)(\theta,s) = \int_{H(\theta,s)} f(x)\mathrm{d}S(x)$ over hyperplanes $H(\theta,s) = \{x \in \mathbb{R}^n : \langle\theta,x\rangle = s\}$, where θ is a normal vector of the hyperplane $H(\theta,s)$, s its oriented distance from the origin and $\mathrm{d}S$ denotes the $n-1$ dimensional surface measure. Most results for the two dimensional case generalize to higher dimensions as well (see, for example [Hel80, Nat01, NW01]).

For example, in three spatial dimensions, the analogon of the filtered backprojection inversion formula (6) reads

$$f(x) = -\frac{1}{8\pi^2}\int_{S^2} (\mathcal{R}f)''(\theta,\langle\theta,x\rangle)\mathrm{d}\theta \qquad \text{for } x \in \mathbb{R}^3\,, \tag{5}$$

where $(\mathcal{R}f)''$ denotes the second derivative of $\mathcal{R}f$ with respect to the second variable. One notices that the inversion formula for the Radon transform in three dimensions looks simpler than its analogon in two dimensions. Moreover, the inversion formula in three dimensions is local in the sense that recovering f at a single point $x \in \mathbb{R}^3$ using (5) only requires values of the Radon transform corresponding to planes which pass through an arbitrarily small neighbourhood of the reconstruction point x. Opposed to that, the 2D inversion formula (4) is non-local: Recovering f at a single point requires knowledge of the integrals of f over all lines in the plane. Note that such a discrepancy also holds in higher dimension: Inversion of the Radon transform is local in every odd dimension and non-local in every even dimension.

2.3 The filtered back-projection algorithm

The filtered backprojection (FBP) algorithm is still the most commonly used reconstruction algorithm for medical x-ray CT, see [PSV09]. It may be seen as a computer implementation of the filtered backprojection inversion formula (4). However,

due to the presence of the derivative, the inversion formula is sensitive to error in the data $\mathcal{R}f$. Such an instability in inherently in the Radon transform and one can show that inversion of the Radon transform is ill-posed of degree $1/2$ (see, [Nat01, Chap. II, Thm. 5.1]). For solving such an ill-posed one has to apply regularization techniques, which replace the exact solution by an approximate but stable one.

It is therefore reasonable to derive the FBP algorithm from the already regularized formula (see Theorem 4)

$$\begin{aligned}(W_b * f)(x) &= \left(\mathcal{R}^\sharp (w_b * \mathcal{R}f)\right)(x) \\ &= \int_{S^1} \int_{\mathbb{R}} w_b(\theta, s)\, (\mathcal{R}f)(\theta, \langle \theta, x\rangle - s)\, \mathrm{d}s\, \mathrm{d}\theta\,, \end{aligned} \tag{6}$$

where $1/b > 0$ is a regularization parameter and $W_b \colon \mathbb{R}^2 \to \mathbb{R}$ and $w_b \colon S^1 \times \mathbb{R} \to \mathbb{R}$ satisfy the dual equation $W_b = \mathcal{R}^\sharp w_b$. In (6) the regularization effect comes from the convolution of the unknown f with a smooth radially symmetric mollifier $W_b \colon \mathbb{R}^2 \to \mathbb{R}$. If the family $\{W_b\}_{b>0}$ is such that $W_b * f \to f$ as $b \to \infty$, then $W_b * f$ is a smooth approximation of the unknown f that can be computed in stable way from the Radon data $\mathcal{R}f$.

The approximate inversion formula (6) is again of the filtered backprojection type. The inner operation is the convolution in the variable s with a smooth kernel and is referred to as the filtering step. The outer operation is refereed to as backprojection and integrates $w_b * \mathcal{R}f$ over all lines that pass through the reconstruction point x. The function w_b is the filtering kernel and requires solving the dual equation $W_b = \mathcal{R}^\sharp w_b$. A variety of filtering kernels can be designed using the following corollary of Theorem 4.

Corollary 5. *Suppose $\Phi \colon [0, \infty) \to \mathbb{R}$ is an integrable function satisfying $0 \le \Phi \le 1$ and $\Phi(\sigma) = 0$ for $\sigma \ge 1$. Further, let W_b denote the inverse Fourier transform of*

$$\hat{W}_b \colon \mathbb{R}^2 \to \mathbb{R} \colon \xi \mapsto \Phi\left(\frac{|\xi|}{b}\right)\,. \tag{7}$$

Then (6) holds with

$$\mathcal{F}_2 w_b\,(\theta, \sigma) = \frac{|\sigma|}{2}\, \Phi\left(\frac{|\sigma|}{b}\right)\,. \tag{8}$$

Proof. Defining W_b, w_b by their Fourier representations (7), (8), Item (b) in Theorem 4 shows $W_b = \mathcal{R}^\sharp w_b$ and therefore (6) follows from Theorem 4 (a). □

The standard FBP algorithm is a straightforward numerical implementation of (6). For that purpose, suppose that only discrete data

$$g_{j,k} := (\mathcal{R}f)(\theta_j, k\Delta s)\,, \qquad \text{for } (j,k) \in \{1, \dots, N\} \times \{-M, \dots, M\}\,,$$

are given, where $\theta_j := (\cos \varphi_j, \sin \varphi_j)$ with $\varphi_j = 2(j-1)\pi/N$ and $\Delta s := 1/M$. The FBP algorithm uses the composite trapezoidal rule for discretizing the inner

integral in (6) at the sampling points which yields

$$\Delta s \sum_{\ell=-M}^{M} w_b(k\Delta s - \ell\Delta s) g_{j,\ell} \simeq \int_{\mathbb{R}} w_b(s-t)\mathcal{R}f(\theta_j, s)\mathrm{d}s\,. \tag{9}$$

Notice that w_b is independent of $\theta \in S^1$ and we have dropped this first argument. The outer integration (backprojection operation) is also discretized with the composite trapezoidal rule evaluated at certain grid points $x \in D$. The required values of $(w_b * \mathcal{R}f)(\theta_j, \cdot)$ evaluated at $\langle \theta_j, x\rangle$ are computed with (9) and subsequent linear interpolation in the second argument.

The most critical step in the FBP algorithm is the discrete convolution in (9), defined by the discrete reconstruction filter

$$(w_b(k\Delta s))_{k=-M,\dots,M}\ ,$$

whose entries are samples of the filtering kernel w_b at the sampling points $k\Delta s$. Based on Corollary 5 one can derive most reconstruction filters used in CT. For example, the strict low pass filter defined by $\Phi(\sigma) = 1$ for $\sigma \in [0,1]$ and $\Phi(\sigma) = 0$ otherwise, yields the filter coefficients

$$w_b(k\Delta s) = \frac{b^2}{2\pi^2}\begin{cases} 1/4 & \text{for } k = 0 \\ -1/(\pi^2 k^2) & \text{for } k \text{ odd} \\ 0 & \text{otherwise}\,. \end{cases}$$

This filter has been proposed in 1971 by Ramachandran and Lakshminarayanan [RL71] and is referred to as *Ram-Lak filter*. The choice $\Phi(\sigma) = \sin(\sigma\pi/2)/(\sigma\pi/2)$ for $\sigma \in [0,1]$ and $\Phi(\sigma) = 0$ otherwise has been proposed in 1974 by Shepp and Logan. The resulting *Shepp-Logan filter coefficients* are given by

$$w_b(k\Delta s) = \frac{b^2}{\pi^4}\frac{1}{1-4k^2}\,.$$

For more details on the FBP algorithm and filter design, see [Dea83, KS01, Nat01].

3 The spherical Radon transform

The classical Radon transform maps a function to its integrals over straight lines. As we have seen in the previous section, it serves as the basis of x-ray CT. In a number of different imaging technologies, there arises a need to reconstruct an unknown function from its integrals over spheres. This leads to the inversion of the so-called spherical Radon transform, which we study in this section.

For an integrable function $f\colon \mathbb{R}^n \to \mathbb{R}$, we define the spherical Radon transform $\mathcal{R}_{\mathrm{sph}}f\colon \mathbb{R}^n \times (0,\infty) \to \mathbb{R}$ by

$$(\mathcal{R}_{\mathrm{sph}}f)(x,t) := \int_{\partial B(x,t)} f(y)\mathrm{d}s(y) \qquad \text{for } (x,t) \in \mathbb{R}^n \times (0,\infty)\,.$$

Here $B(x,t) := \{y \in \mathbb{R}^n : |x-y| < t\}$ is the open n-dimensional ball of radius $t > 0$ centered at x with respect to the usual Euclidean norm, $\partial B(x,t)$ is its boundary, and $\mathrm{d}s$ denotes the standard surface measure. For $n = 2$, one also calls $\mathcal{R}_{\mathrm{sph}}$ the circular Radon transform.

The spherical Radon transform arises, for example, in photoacoustic tomography (PAT) [BBMG+07, FR09, KK08, XW06], sound navigation and ranging (SONAR) [BF09, QRS11], synthetic aperture radar (SAR) [And88, RP03], ultrasound tomography [Nor80, NL81], and seismic imaging [BCSJ01, Faw85]. In the following subsection, we show how the 2D and 3D spherical Radon transforms arise in the quite recently developed PAT.

3.1 Photoacoustic tomography

PAT is based on the so-called photoacoustic effect. When short pulses of non-ionising electromagnetic energy are delivered into a biological (semi-transparent) tissue, then parts of the electromagnetic energy become absorbed. The absorbed energy leads to a nonuniform thermoelastic expansion (depending on the tissue structure), which in turn generates an ultrasonic wave. These waves are detected by a measurement device on the boundary of the tissue (see Figure 3). The mathematical task in PAT is to reconstruct the spatially varying absorption coefficient using these measurements.

While x-ray CT has a rather low contrast in soft tissues, the electromagnetic absorption coefficient at some lower frequencies shows significantly higher variation. PAT therefore provides good imaging contrast in soft tissues making it a very promising technique for detecting various types of early cancer, such as breast cancer or skin melanoma. In 1998, the first clinical prototype of a PAT scanner for breast screeing has been developed by Kruger [KSK02]. Various practical aspects of PAT are discussed in [XW06].

The reconstruction of the absorption coefficient in an object under investigation from the measured acoustic waves on the boundary of the object requires a mathematical model for the relationship between the absorption coefficient and the boundary acoustic waves. Below we briefly review such a model, following the approach presented in [Hal10, HSS05, SGG+09].

Mathematical modeling

Suppose the object to be investigated is supported in a domain $\Omega \subset \mathbb{R}^3$ that is illuminated with a short pule of electromagnetic energy near the visible range. We denote by $I(x,t) = J(x)j(t)$ the intensity of the electromagnetic energy at location $x \in \mathbb{R}^3$ and time $t \in \mathbb{R}$ with $J(x)$ being the spatial and $j(t)$ the temporal intensity distribution. The rate of absorbed electromagnetic energy is described by the absorbed electromagnetic power $r(x,t) = \mu_{\mathrm{abs}}(x)\, I(x,t)$, where $\mu_{\mathrm{abs}}(x)$ is the spatially varying absorption coefficient. The rate of absorbed energy causes a temperature change which is in turn related to an increase of acoustic pressure $p(x,t)$.

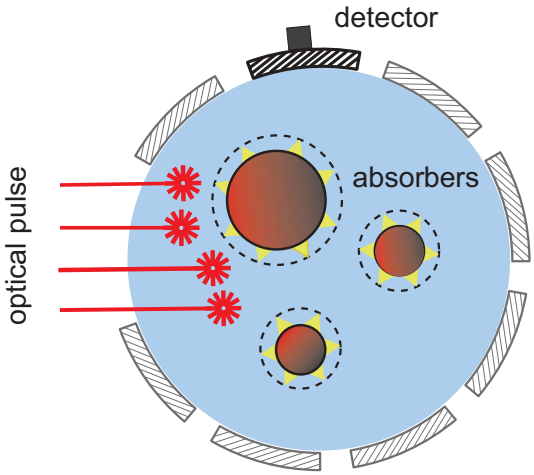

Figure 3: Illustration of PAT. Electromagnetic pulses are delivered into the tissue. Ultrasound detectors measure the generated acoustic waves on the boundary.

Since the pulse duration is very short, the heat transfer by conduction can be neglected [Tam86].

Employing the linearised equations of fluid dynamics (for details, see [Hal10] or [SGG+09, Section 1.5]) one shows

$$\frac{1}{v_s(x)^2}\frac{\partial^2 p(x,t)}{\partial t^2} - \Delta p(x,t) = f(x)\frac{dj}{dt}(t)\,, \qquad \text{for } (x,t) \in \mathbb{R}^3 \times \mathbb{R}\,, \tag{10}$$

with $f(x) = I(x)\beta(x)\mu_{\text{abs}}(x)/C_p(x)$. Here $C_p(x)$ is the specific heat capacity, $\beta(x)$ is the thermal expansion coefficient at constant pressure and $v_s(x)$ is the speed of sound. The wave equation (10) is augmented with the initial conditions $p(x,t) = 0$ for $t < 0$, reflecting the fact that there is no acoustic pressure before the illumination starts at $t = 0$.

In the following we assume that the sound speed $v_s = v_s(x)$ is constant and after rescaling we can assume that v_s equals one, and that $j(t)$ is approximates the one-dimensional δ-distribution. Then, by Duhamel's principle [Eva98, p. 81], the solution of (10) coincides, for $t > 0$, with the solution of the initial value problem

$$\begin{cases} \left(\partial_t^2 - \Delta\right) p(x,t) = 0 & \text{for } (x,t) \in \mathbb{R}^3 \times (0,\infty) \\ p(x,0) = f(x) & \text{for } x \in \mathbb{R}^3 \\ \dfrac{\partial p}{\partial t}(x,0) = 0 & \text{for } x \in \mathbb{R}^3\,. \end{cases} \tag{11}$$

The aim of PAT is to reconstruct the function $f(x)$, proportional to the absorption coefficient, from measurements of the solution of (11) taken outside of the support of f. The particular mathematical problem to solve, also depends on the way how the acoustic signals are measured. Different measurement setups lead to different mathematical problems. Below we shortly review the concepts of point-like and

linear integrating measurement setups, which yield to the inversion of the spherical Radon transform in three and two dimensions, respectively.

Point measurement: 3D spherical Radon transform

In the standard measurement procedure used in PAT, small piezoelectric detectors are placed on the object's boundary and they record arriving acoustic waves there (see Figure 4 left). These detectors can be seen as an approximation to idealised point detectors that record the solution of (11) pointwise on the boundary $\partial\Omega$.

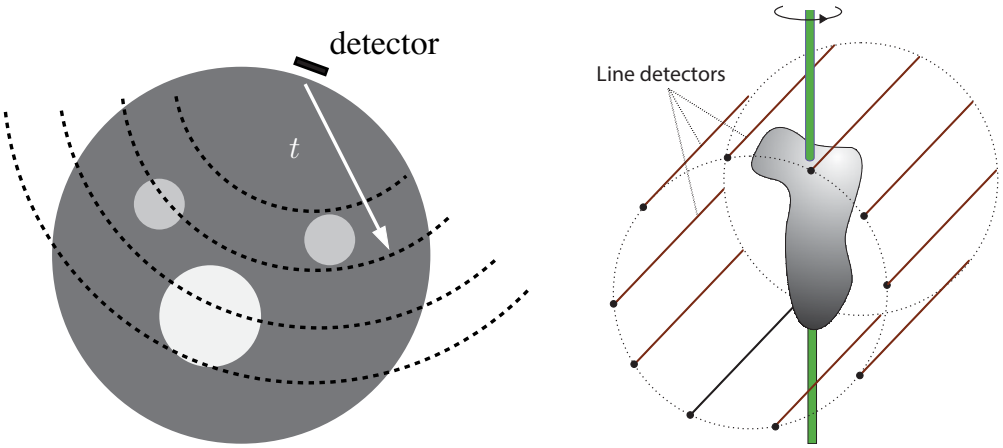

Figure 4: LEFT: The data measured by small piezoelectric detectors can provide integrals of the unknown function over spheres. RIGHT: The array of the line detectors measures the acoustic waves during the rotation around the object.

The well known explicit expression for the solution of the initial value problem (11) in terms of the three-dimensional spherical Radon transform (see, for example, [Eva98, page 72]) reads

$$p(x,t) = \frac{\partial}{\partial t}\left[\frac{1}{4\pi t}(\mathcal{R}_{\text{sph}}f)(x,t)\right] \qquad \text{for } (x,t) \in \mathbb{R}^3 \times (0,\infty)\,.$$

Integrating this expression with respect to t yields

$$(\mathcal{R}_{\text{sph}}f)(x,t) = 4\pi t \int_0^t p(x,s)\mathrm{d}s.$$

Thus, the reconstruction of the initial pressure distribution from measurements of point detectors on the object boundary yield to the problem of inverting the spherical Radon with centers restricted to $\partial\Omega$.

Line measurement: 2D spherical Radon transform

Since in practice every acoustic detector has a finite size, the algorithms that are based on the assumption of point-like measurements produce blurred reconstruction (see [HZ10, RHN+14, XW03]). In order to partially compensate for this effect, in [HSBP04] it is suggested to use large planar detectors that measure integrals of the acoustic pressure over planes. As a further development in [BHP+05, PNHB07b] so-called line detectors have bee proposed that use integrals of the acoustic pressure over lines and which can be efficiently realized in practice.

The measurement setup with line detectors is as follows. The devices are put into an array of detectors that are parallel to each other, and this array is rotated around a single axis (Figure 4 right). Let p be the solution of (11) and assume that the line detectors are parallel to the direction $e_1 := (1,0,0)$. Also, let us write $x = (x_1, x')$ with $x_1 \in \mathbb{R}$ and $x' \in \mathbb{R}^2$, and denote by

$$\bar{p}(x',t) = \int_{\mathbb{R}} p(x_1,x',t)\mathrm{d}x_1 \qquad \text{for } (x',t) \in \mathbb{R}^2 \times (0,\infty)$$

the pressure values integrated in direction e_1. It is not hard to show that the integrated pressure $\bar{p}$ satisfies the following two dimensional initial value problem (see, for example, [BBMG+07])

$$\begin{cases} \left(\partial_t^2 - \Delta\right)\bar{p}(x',t) = 0 & \text{for } (x',t) \in \mathbb{R}^2 \times (0,\infty) \\ \bar{p}(x',0) = \bar{f}(x') & \text{for } x' \in \mathbb{R}^2 \\ \dfrac{\partial \bar{p}}{\partial t}(x',0) = 0 & \text{for } x' \in \mathbb{R}^2\,. \end{cases} \tag{12}$$

Here $\bar{f}(x') := \int_{\mathbb{R}} f(x_1,x')\mathrm{d}x_1$ is the linear projection of f in direction e_1. Data of line detectors provide values $p(x',t)$ for certain measurement positions x' outside of the support of f'. Note that having obtained the linear projections $\bar{f}$ from different directions, the reconstruction of f can be obtained from the inversion of the classical (linear) Radon transform studied in Section 2.

Similar to its three dimensional counterpart, the two dimensional reconstruction problem based on (12) can be recast as the problem of inverting the spherical Radon transform: Note that the solution of the 2D wave equation is given by (see, for example, [Joh82, Equation (1.24a)])

$$\bar{p}(x',t) = \frac{1}{2\pi}\frac{\partial}{\partial t}\int_0^t \frac{\left(\mathcal{R}_{\mathrm{sph}}\bar{f}\right)(x',r)}{\sqrt{t^2-r^2}}\,\mathrm{d}r \qquad \text{for } (x',t) \in \mathbb{R}^2 \times (0,\infty)\,.$$

Application of standard tools for solving Abel type integral equations (see, for example, [GV91, Nat01]) yields the following expression for $\mathcal{R}_{\mathrm{sph}}\bar{f}$ in terms of the data values:

$$\left(\mathcal{R}_{\mathrm{sph}}\bar{f}\right)(x',r) = 4r\int_0^r \frac{\bar{p}(x',t)}{\sqrt{r^2-t^2}}\mathrm{d}t\,.$$

Consequently, PAT with integrating line detectors yields to the problem of reconstructing $\bar{f}$ from its circular Radon transform, which is the 2D analogon of the 3D reconstruction problem in PAT using point-like measurements.

3.2 Inversion formulas

Exact inversion formulas for the spherical Radon transform are currently known for boundaries of special domains, including spheres, cylinders and hyperplanes. Recently explicit inversion formulas for elliptic domains started to appear in the literature [AFMS13, Hal13, Hal14a, Hal14b, Nat12, Pal12]. In [HP14], we showed that the formula [Hal13] for elliptic domains in 2D is also exact for parabolic domains.

Exemplarily we present inversion formulas from [FHR07] for the circular Radon transform with centers centers of integration restricted to a circle, and the inversion formulas from [Hal13] for boundaries of ellipses, which are also exact for circles.

Recall that $B(x,t) \subset \mathbb{R}^2$ denotes the open ball of radius $t > 0$ centered at x. For a general domain $\Omega \subset \mathbb{R}^2$, we denote by $C_c^\infty(\Omega)$ the set of all smooth functions $f\colon \mathbb{R}^2 \to \mathbb{R}$ that are compactly supported in Ω.

Theorem 6 (Inversion formulas of [FHR07])**.** *Let $D_R := B(0,R) \subset \mathbb{R}^2$ denote the disc of radius R centered at the origin, suppose that $f \in C_c^\infty(D_R)$ and extend $(\mathcal{R}_{\mathrm{sph}} f)(x,t)$ as an even function in the second variable t.*

Then, for all $x_0 \in D_R$, the function f can be recovered from $\mathcal{R}_{\mathrm{sph}} f$ with the help of the following formulas:

$$f(x_0) = \frac{1}{4\pi^2 R} \int_{\partial D_R} \int_{-2R}^{2R} \frac{(t\partial_t t^{-1} \mathcal{R}_{\mathrm{sph}} f)(x,t)}{|x_0 - x| - t} \,\mathrm{d}t\mathrm{d}s(x)\,,$$

$$f(x_0) = \frac{1}{4\pi^2 R} \int_{\partial D_R} |x_0 - x| \int_{-2R}^{2R} \frac{(\partial_t t^{-1} \mathcal{R}_{\mathrm{sph}} f)(x,t)}{|x_0 - x| - t} \,\mathrm{d}t\mathrm{d}s(x)\,,$$

where the inner integrals are taken in the principal value sense.

Note that many researchers believed that exact reconstruction formulas in 2D exist only for circles and lines. However recently, it was shown in [Nat12] that the so-called universal back-projection formula from [XW05] is theoretically exact for ellipsoids in $\mathbb{R}^3$. In [Hal13] such formulas have been derived for ellipses in $\mathbb{R}^2$. The formulas of [Nat12, Hal13] in fact can be used for arbitrary bounded convex domains. However, in this case the formulas do not recover the underlying function exactly and give an error. In both papers [Nat12, Hal13], the corresponding error term has been explicitly derived. The results of [Nat12, Hal13] have been generalized to arbitrary dimension in [Hal14b]. Note that for the special case of spherical domains the formulas of [Hal14b] also coincide with the formulas of [Kun07]. Very recently one of the formulas of [FHR07, FPR04] has been generalized to elliptical domains in [Salar, Hal14a].

The inversion formulas from [Hal13] read as follows.

Theorem 7 (Inversion formulas of [Hal13])**.** *Suppose $\Omega \subset \mathbb{R}^2$ is a circular or elliptical domain and let $f \in C_c^\infty(\Omega)$. Then, for all $x_0 \in \Omega$, the following holdf:*

$$f(x_0) = \frac{1}{2\pi^2} \nabla_{x_0} \cdot \int_{\partial\Omega} \nu_x \int_0^\infty \frac{\mathcal{R}_{\mathrm{sph}} f(x,t)}{t^2 - |x_0 - x|^2} \,\mathrm{d}t\mathrm{d}s(x)\,,$$

$$f(x_0) = \frac{1}{2\pi^2} \int_{\partial\Omega} \langle \nu_x, x_0 - x \rangle \int_0^\infty \frac{(\partial_t t^{-1} \mathcal{R}_{\text{sph}}) f(x,t)}{t^2 - |x_0 - x|^2} \, \mathrm{d}t \mathrm{d}s(x) \,. \tag{13}$$

Here ν_x denotes the outwards pointing unit normal to $\partial\Omega$ and the inner integrals are understood in the principal value sense.

In [HP14], we showed that the second formula in the above theorem is also exact for the case where Ω is a parabolic domain.

If one has the pure wave data $\bar{p}(x,t)$, i.e. the solution of the initial value problem (12) is given on the boundary of an elliptic or parabolic domain Ω, then the corresponding initial pressure distribution can be recovered by means of the following formula (see [BBMG+07, Hal13, HP14]):

$$\bar{f}(x_0) = \frac{1}{\pi} \int_{\partial\Omega} \langle \nu_x, x_0 - x \rangle \int_{|x_0 - x|}^\infty \frac{(\partial_t t^{-1} \bar{p})(x,t)}{\sqrt{t^2 - |x_0 - x|^2}} \, \mathrm{d}t \mathrm{d}s(x), \tag{14}$$

for any reconstruction point $x_0 \in \Omega$.

3.3 Numerical results

The formulas (13), (14) can be implemented as outlined in [BBMG+07, FHR07]. For illustration, we present numerical results for the recovery from the wave data (the solution (12)) in two spatial dimensions. We consider a function $\bar{f} \colon \mathbb{R}^2 \to \mathbb{R}$ given by the phantom shown in Figure 5. The same phantom has been used for testing the numerical performance of the reconstruction formulas in [BBMG+07, Hal13, HP14]. The support of the corresponding function $\bar{f}$ is included in the parabolic domain

$$P = \left\{ (a,b) \in \mathbb{R}^2 \mid b > 0.6\, a^2 \ - 1 \right\}.$$

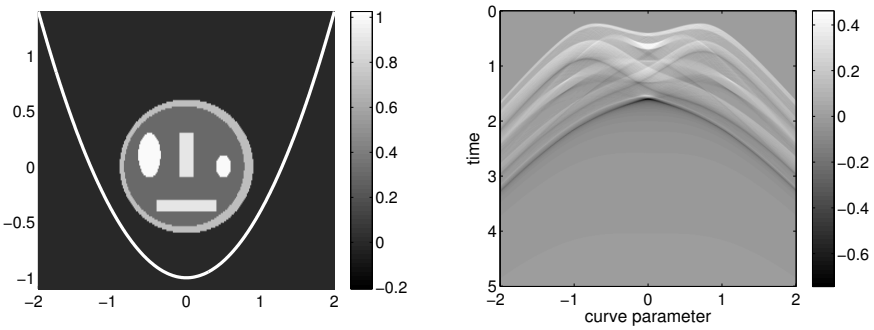

Figure 5: LEFT: The phantom in the parabolic domain P that is used for the numerical results. RIGHT: The simulated wave data $\bar{p}$ on the recording curve Γ_1. The variable a is considered as the curve parameter.

Figure 6: The numerical reconstructions $\bar{f}_i$, $i = 1, 2, 3$ (from left to right) on the reconstruction subdomain $\bar{P}$. The gray scale is as for the phantom of Figure.

For the numerical realization of formula (14), one first has to replace the integral over ∂P by the integral over a curve with finite length. We take the following integration curves:

$$\Gamma_i = \left\{(a, b) \in \mathbb{R}^2 \mid b = 0.6\, a^2 - 1,\ a \in [-a_i, a_i]\right\} \qquad \text{for } i = 1, 2, 3\,,$$

with $a_1 = 2$, $a_2 = 4$, $a_3 = 6$, respectively. The simulated wave data $\bar{p}$ on the curve Γ_1 is presented in Figure 5.

Let us present the reconstructions $\bar{f}_i(x)$ that are obtained by the numerical realization of formula (14) where the integration curve ∂P is replaced by Γ_i. These reconstructions on the reconstruction subdomain (the set where the inversion formula is evaluated)

$$\bar{P} = \left\{(a, b) \in \mathbb{R}^2 \mid 0.6\, a^2 - 1 < b < 0.6 \cdot 2^2 - 1,\ a \in (-2, 2)\right\}$$

at the points $\{0.015(i, j) : (i, j)\} \in \mathbb{Z}^2\} \cap \bar{P}$ are shown in Figure 6. The time step size for the inner integral in (14) is taken 0.01. The integration curves are discretized such that the distance between two consecutive points is in the interval $[0.0099, 0.0101]$. The numbers of the discretization points on the considered integration curves are the following: 659, 2166, 4617.

The reconstruction errors for the finite parabolas Γ_i decrease as the length of Γ_i increases. It should be noted that the reconstruction problem in the case of the open curves Γ_i corresponds to the so-called limited view problem [Kun08, PNB09, PNHB07a, XWAK04]. For each reconstruction point inside the reconstruction subdomain $\bar{P}$ there is a considerable set of directions for which the boundary wave data is missing, which is known to create reconstruction artefacts. We refer to [HP14] for the comparison with the reconstructions on closed parabolas and ellipses.

4 Concluding remarks

In this note we have given a brief introduction to CT and presented mathematical results serving as basis of FBP reconstruction algorithms. We thereby focused on two prime examples, namely classic x-ray CT and the more recent PAT. These

applications require inversion of the classical Radon transform and the spherical Radon transform, respectively. The most common algorithm for these applications is the filtered backprojection (FBP) algorithm, which implements exact inversion formulas we presented above.

Note that we mainly focused on the development of FBP algorithms for inverting Radon type transforms. In some tomographic applications iterative reconstruction algorithms are more common. For example, in single photo emission tomography (SPECT), the statistical noise is an important issue and iterative reconstruction algorithms based on a maximum likelihood minimization are favoured. A prominent iterative procedures for maximum likelihood minimization is the EM algorithm (expectation maximisation algorithm) of Dempster, Laird and Rubin [DLR77], which has been introduced to computed tomography in [SV82, VSK85]. Note that also the first reconstruction algorithms in x-ray CT have been of iterative nature (see [Hou73, GBH70]). The used algorithm became popular known under the name ART (algebraic reconstruction technique) and was later (see [GKK+74]) identified as Kaczmarz's iterative procedure [Kac37] for the solution of systems of linear equations. See, for example, [Her09, Nat01, NW01] for more details on the use of iterative reconstruction algorithm in CT.

Finally, note that some tomographic applications are better modelled as parameter identification problems for partial differential equations. This often yields to nonlinear inverse problems. See [EHN96, Isa98, IVT02, Mor93, SGG+09, TA77] for general solution methods approaching such type of problems.

References

[AFMS13] M. Ansorg, F. Filbir, W. R. Madych, and R. Seyfried. Summability kernels for circular and spherical mean data. *Inverse Problems*, 29(1):015002, 2013.

[And88] L.-E. Andersson. On the determination of a function from spherical averages. *SIAM J. Math. Anal.*, 19(1):214–232, 1988.

[AY02] L. Antonuk and M. Yaffe, editors. *Medical Imaging 2002: Physics of Medical Imaging*, volume 4682 of *Proceedings of SPIE*, 2002.

[BBMG+07] P. Burgholzer, J. Bauer-Marschallinger, H. Grün, M. Haltmeier, and G. Paltauf. Temporal back-projection algorithms for photoacoustic tomography with integrating line detectors. *Inverse Probl.*, 23(6):S65–S80, 2007.

[BCSJ01] N. Bleistein, J. K. Cohen, and J. W. Stockwell Jr. *Mathematics of multidimensional seismic imaging, migration, and inversion*, volume 13 of *Interdisciplinary Applied Mathematics*. Springer, New York, 2001.

[Bey95] G. Beylkin. On the fast Fourier transform of functions with singularities. *Applied and Computational Harmonic Analysis*, 2(4), 1995.

[BF09] A. Beltukov and D. Feldman. Identities among Euclidean Sonar and Radon transforms. *Adv. in Appl. Math.*, 42(1):23–41, 2009.

[BHP+05] P. Burgholzer, C. Hofer, G. Paltauf, M. Haltmeier, and O. Scherzer. Thermoacoustic tomography with integrating area and line detectors. *IEEE Trans. Ultrason., Ferroeletr., Freq. Control*, 52(9):1577–1583, September 2005.

[Cor63] A. M. Cormack. Representation of a function by its line integrals, with some radiological applications. *J. App. Phys.*, 34(9):2722–2727, 1963.

[Dea83] S. R. Deans. *The Radon transform and some of its Applications*. John Wiley & Sons, New York, 1983.

[DLR77] A. P Dempster, N. M. Laird, and D. B. Rubin. Maximum likelihood from incomplete data via the em algorithm. *J. Roy. Statist. Soc. Ser. B*, pages 1–38, 1977.

[DR93] A. Dutt and V. Rokhlin. Fast Fourier transforms for nonequispaced data. *SIAM J. Sci. Comput.*, 14(6), 1993.

[EHN96] H. W. Engl, M. Hanke, and A. Neubauer. *Regularization of inverse problems*, volume 375 of *Mathematics and its Applications*. Kluwer Academic Publishers Group, Dordrecht, 1996.

[Eva98] L. C. Evans. *Partial Differential Equations*, volume 19 of *Graduate Studies in Mathematics*. American Mathematical Society, Providence, RI, 1998.

[Faw85] J. A. Fawcett. Inversion of n-dimensional spherical averages. *SIAM J. Appl. Math.*, 45(2):336–341, 1985.

[Fes07] J. A Fessler. On NUFFT-based gridding for non-cartesian MRI. *Journal of Magnetic Resonance*, pages 191–195, 2007.

[FHR07] D. Finch, M. Haltmeier, and Rakesh. Inversion of spherical means and the wave equation in even dimensions. *SIAM J. Appl. Math.*, 68(2):392–412, 2007.

[Fou03] K. Fourmont. Non-equispaced fast Fourier transforms with applications to tomography. *J. Fourier Anal. Appl.*, 9(5):431–450, 2003.

[FPR04] D. Finch, S. K. Patch, and Rakesh. Determining a function from its mean values over a family of spheres. *SIAM J. Math. Anal.*, 35(5):1213–1240, 2004.

[FR09] D. Finch and Rakesh. Recovering a function from its spherical mean values in two and three dimensions. In L. V. Wang, editor, *Photoacoustic imaging and spectroscopy*, chapter 7, pages 77–88. CRC Press, 2009.

[Fun13] P. Funk. Über flächen mit lauter geschlossenen geodätischen linien. *Math. Ann.*, 74(2):278–300, 1913.

[GBH70] R. Gordon, R. Bender, and G. T. Herman. Algebraic reconstruction techniques (art) for three-dimensional electron microscopy and x-ray photography. *J. Theor. Biol.*, 29(3):471–481, 1970.

[GGF00] D. Gottleib, B. Gustafsson, and P. Forssen. On the direct fourier method for computer tomography. *IEEE Trans. Med. Imag.*, 19(3):223–232, 2000.

[GKK+74] R. B. Guenther, C. W. Kerber, E. K. Killian, K. T. Smith, and S. L. Wagner. Reconstruction of objects from radiographs and the location of brain tumors. *Proc. Natl. Acad. Sci. U.S.A.*, 71(12):4884–4886, 1974.

[GL04] L. Greengard and J. Lee. Accelerating the nonuniform fast Fourier transform. *SIAM Rev.*, 46(3):443–454 (electronic), 2004.

[GV91] R. Gorenflo and S. Vessella. *Abel integral equations*, volume 1461 of *Lecture Notes in Mathematics*. Springer-Verlag, Berlin, 1991. Analysis and applications.

[Hal10] M. Haltmeier. *Mathematical Methods in Photoacoustic Image Reconstruction*. Habilitation, University of Vienna, Austria, Vienna, February 2010.

[Hal13] M. Haltmeier. Inversion of circular means and the wave equation on convex planar domains. *Comput. Math. Appl.*, 65(7):1025–1036, 2013.

[Hal14a] M. Haltmeier. Exact reconstruction formula for the spherical mean Radon transform on ellipsoids. arXiv:1404.3935 [math.AP], 2014.

[Hal14b] M. Haltmeier. Universal inversion formulas for recovering a function from spherical means. *SIAM J. Math. Anal.*, 46(1):214–232, 2014.

[Hel80] S. Helgason. *The Radon Transform*, volume 5 of *Progress in Mathematics*. Birkhäuser, Boston, 1980.

[Her09] G. T. Herman. *Fundamentals of computerized tomography*. Advances in Pattern Recognition. Springer, Dordrecht, second edition, 2009. Image reconstruction from projections.

[Hou73] G. N. Hounsfield. Computerised transverse axial scanning (tomography). Part 1: Description of system. *Brit. J. Radiology*, 46(552):1016–1022, 1973.

[HP14] M. Haltmeier and S. Pereverzyev Jr. Recovering a function from circular means or wave data on the boundary of parabolic domains. Technical report, University of Innsbruck, Department of Mathematics, Applied Mathematics Group, 2014. Preprint Nr. 12.

[HSBP04] M. Haltmeier, O. Scherzer, P. Burgholzer, and G. Paltauf. Thermoacoustic computed tomography with large planar receivers. *Inverse Probl.*, 20(5):1663–1673, 2004.

[HSS05] M. Haltmeier, T. Schuster, and O. Scherzer. Filtered backprojection for thermoacoustic computed tomography in spherical geometry. *Math. Methods Appl. Sci.*, 28(16):1919–1937, 2005.

[HZ10] M. Haltmeier and G. Zangerl. Spatial resolution in photoacoustic tomography: Effects of detector size and detector bandwidth. *Inverse Probl.*, 26(12):125002, 2010.

[Isa98] V. Isakov. *Inverse Problems for Partial Differential Equations*, volume 127. Springer Verlag, New York, 1998. Applied Mathematical Sciences.

[IVT02] V. K. Ivanov, V. V. Vasin, and V. P. Tanana. *Theory of linear ill-posed problems and its applications*. Inverse and Ill-posed Problems Series. VSP, Utrecht, second edition, 2002. Translated and revised from the 1978 Russian original.

[Joh82] F. John. *Partial Differential Equations*, volume 1 of *Applied Mathematical Sciences*. Springer Verlag, New York, fourth edition, 1982.

[Kac37] S. Kaczmarz. Angenäherte Auflösung von Systemen linearer Gleichungen. *Bull. Int. Acad. Pol. Sci. Lett. A*, 35:355–357, 1937.

[KKP09] J. Keiner, S. Kunis, and D. Potts. Using NFFT 3—a software library for various nonequispaced fast Fourier transforms. *ACM Trans. Math. Software*, 36(4): Article No. 19, 2009.

[KK08] P. Kuchment and L. A. Kunyansky. Mathematics of thermoacoustic and photoacoustic tomography. *European J. Appl. Math.*, 19:191–224, 2008.

[KS01] A. C. Kak and M. Slaney. *Principles of Computerized Tomographic Imaging*, volume 33 of *Classics in Applied Mathematics*. Society for Industrial and Applied Mathematics (SIAM), Philadelphia, PA, 2001.

[KSK02] R. A. Kruger, K. M. Stantz, and W. L. Kiser. Thermoacoustic CT of the breast. In *[AY02]*, pages 521–525, 2002.

[Kuc14] P. Kuchment. *The Radon transform and medical imaging*, volume 85 of *CBMS-NSF Regional Conference Series in Applied Mathematics*. Society for Industrial and Applied Mathematics (SIAM), Philadelphia, PA, 2014.

[Kun07] L. A. Kunyansky. Explicit inversion formulae for the spherical mean Radon transform. *Inverse Probl.*, 23(1):373–383, 2007.

[Kun08] L. A. Kunyansky. Thermoacoustic tomography with detectors on an open curve: an efficient reconstruction algorithm. *Inverse Problems*, 24(5):055021, 2008.

[Mor93] V. A. Morozov. *Regularization Methods for Ill-Posed Problems*. CRC Press, Boca Raton, 1993.

[Nat01] F. Natterer. *The Mathematics of Computerized Tomography*, volume 32 of *Classics in Applied Mathematics*. SIAM, Philadelphia, 2001.

[Nat12] F. Natterer. Photo-acoustic inversion in convex domains. *Inverse Probl. Imaging*, 6(2):1–6, 2012.

[NL81] S. J. Norton and M. Linzer. Ultrasonic reflectivity imaging in three dimensions: Exact inverse scattering solutions for plane, cylindrical and spherical apertures. *IEEE Trans. Biomed. Eng.*, 28(2):202–220, 1981.

[Nor80] S. J. Norton. Reconstruction of a two-dimensional reflecting medium over a circular domain: Exact solution. *J. Acoust. Soc. Amer.*, 67(4):1266–1273, 1980.

[NW01] F. Natterer and F. Wübbeling. *Mathematical Methods in Image Reconstruction*, volume 5 of *Monographs on Mathematical Modeling and Computation*. SIAM, Philadelphia, PA, 2001.

[O'S85] J. D. O'Sullivan. A fast sinc function gridding algorithm for Fourier inversion in computer tomography. *IEEE Trans. Med. Imag.*, 4:200–207, 1985.

[Pal12] V. P. Palamodov. A uniform reconstruction formula in integral geometry. *Inverse Probl.*, 28(6):065014, 2012.

[PNB09] G Paltauf, R Nuster, and P Burgholzer. Weight factors for limited angle photoacoustic tomography. *Phys. Med. Biol.*, 54(11):3303, 2009.

[PNHB07a] G. Paltauf, R. Nuster, M. Haltmeier, and P. Burgholzer. Experimental evaluation of reconstruction algorithms for limited view photoacoustic tomography with line detectors. *Inverse Probl.*, 23(6):S81–S94, 2007.

[PNHB07b] G. Paltauf, R. Nuster, M. Haltmeier, and P. Burgholzer. Photoacoustic tomography using a Mach-Zehnder interferometer as an acoustic line detector. *App. Opt.*, 46(16):3352–3358, 2007.

[PST01] D. Potts, G. Steidl, and M. Tasche. Fast Fourier transforms for nonequispaced data: a tutorial. In *Modern sampling theory*, Appl. Numer. Harmon. Anal., pages 247–270. Birkhäuser Boston, Boston, MA, 2001.

[PSV09] X. Pan, E. Y. Sidky, and M. Vannier. Why do commercial ct scanners still employ traditional, filtered back-projection for image reconstruction? *Inverse Probl.*, 25(12):123009, 2009.

[QRS11] E. T. Quinto, A. Rieder, and T. Schuster. Local inversion of the sonar transform regularized by the approximate inverse. *Inverse Problems*, 27(3):035006, 18, 2011.

[Rad17] J. Radon. Über die Bestimmung von Funktionen durch ihre Integralwerte längs gewisser Mannigfaltigkeiten. *Ber. Verh. Kön. Sächs. Ges. Wiss. Leipzig Math. Phys. Kl.*, 69:262–277, 1917.

[RHN+14] H. Roitner, M. Haltmeier, R. Nuster, D. P O'Leary, T. Berer, G. Paltauf, H. Grün, and P. Burgholzer. Deblurring algorithms accounting for the finite detector size in photoacoustic tomography. *J. Biomed. Opt.*, 19(5):056011, 2014.

[RL71] G. N. Ramachandran and F. Lakshminarayanan. Three–dimensional reconstruction from radiographs and electron micrographs: Application of convolutions instead of fourier transforms. *Proc. Nat. Acad. Sci. USA*, 68(9):2236–2240, 1971.

[RP03] N. J. Redding and T. M. Payne. Inverting the spherical Radon transform for 3d SAR image formation. In *Proc. Int. Radar Conf.*, pages 466–471, 2003.

[Salar] Y. Salman. An inversion formula for the spherical mean transform with data on an ellipsoid in two and three dimensions. *J. Math. Anal. Appl.*, 2014 (to appear).

[SGG+09] O. Scherzer, M. Grasmair, H. Grossauer, M. Haltmeier, and F. Lenzen. *Variational methods in imaging*, volume 167 of *Applied Mathematical Sciences*. Springer, New York, 2009.

[ST95] H. Schomberg and J. Timmer. The gridding method for image reconstruction by Fourier transformation. *IEEE Trans. Med. Imag.*, 14:596–607, 1995.

[SV82] L. A. Shepp and Y. Vardi. Maximum likelihood reconstruction for emission tomography. *IEEE Trans. Med. Imag.*, 1(2):113–122, 1982.

[TA77] A. N. Tikhonov and V. Y. Arsenin. *Solutions of Ill-Posed Problems*. John Wiley & Sons, Washington, D.C., 1977.

[Tam86] A. C. Tam. Applications of photoacoustic sensing techniques. *Rev. Modern Phys.*, 58(2):381–431, 1986.

[VSK85] Y. Vardi, L. A. Shepp, and L. Kaufman. A statistical model for positron emission tomography. *J. Amer. Statist. Assoc.*, 80(389):8–37, 1985. With discussion.

[XW03] M. Xu and L. V. Wang. Analytic explanation of spatial resolution related to bandwidth and detector aperture size in thermoacoustic or photoacoustic reconstruction. *Phys. Rev. E*, 67(5):0566051–05660515 (electronic), 2003.

[XW05] M. Xu and L. V. Wang. Universal back-projection algorithm for photoacoustic computed tomography. *Phys. Rev. E*, 71(1):0167061–0167067, 2005.

[XW06] M. Xu and L. V. Wang. Photoacoustic imaging in biomedicine. *Rev. Sci. Instruments*, 77(4):041101 (22pp), 2006.

[XWAK04] Y. Xu, L. V. Wang, G. Ambartsoumian, and P. Kuchment. Reconstructions in limited-view thermoacoustic tomography. *Med. Phys.*, 31(4):724–733, 2004.